JACS
JOURNAL OF THE AMERICAN CHEMICAL SOCIETY
pubs.acs.org/JACS
Article

Oligodimethylsiloxane-Oligoproline Block Co-Oligomers: the Interplay between Aggregation and Phase Segregation in Bulk and Solution

Brigitte A.G. Lamers, Andreas Herdlitschka, Tobias Schnitzer, Mathijs F.J. Mabesoone, Sandra M.C. Schoenmakers, Bas F.M. de Waal, Anja R.A. Palmans, Helma Wennemers,* and E.W. Meijer*

Cite This: J. Am. Chem. Soc. 2021, 143, 4032−4042

Read Online

ACCESS | Metrics & More | Article Recommendations | Supporting Information

ABSTRACT: Discrete block co-oligomers (BCOs) assemble into highly ordered nanostructures, which adopt a variety of morphologies depending on their environment. Here, we present a series of discrete oligodimethylsiloxane-oligoproline (*o*DMS-*o*Pro) BCOs with varying oligomer lengths and proline end-groups, and study the nanostructures formed in both bulk and solution. The conjugation of oligoprolines to apolar siloxanes permits a study of the aggregation behavior of oligoproline moieties in a variety of solvents, including a highly apolar solvent like methylcyclohexane. The apolar solvent is more reminiscent of the polarity of the siloxane bulk, which gives insights into the supramolecular interactions that govern both bulk and solution assembly processes of the oligoproline. This extensive structural characterization allows the bridging of the gap between solution and bulk assembly. The interplay between the aggregation of the oligoproline block and the phase segregation induced by the siloxane drives the assembly. This gives rise to disordered, micellar microstructures in apolar solution and crystallization-driven lamellar nanostructures in the bulk. While most di- and triblock co-oligomers adopt predictable morphological features, one of them, *o*DMS$_{15}$-*o*Pro$_6$-NH$_2$, exhibits pathway complexity leading to gel formation. The pathway selection in the complex interplay between aggregation and phase segregation gives rise to interesting material properties.

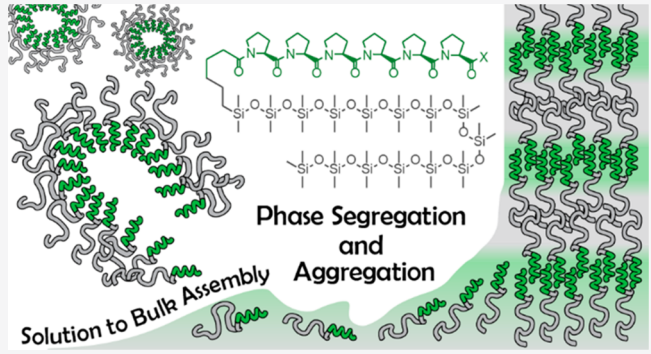

INTRODUCTION

Amphiphilic peptide aggregates have been studied in great detail and a large variety of structures can be obtained depending on the peptide and whether it is in bulk or solution.[1] Larger amphiphilic structures are formed by the conjugation of a flexible polymer coil to a stiff peptide rod, forming a peptide-based block copolymer (BCP) that aggregates in solution as a result of (un)favorable interactions with solvent molecules.[2−4] In polar solvents, the helical, stiff peptide rods assemble and a hydrophilic coil solubilizes the colloids while an apolar coil is needed for the assembly in apolar solvents.[5−8] Studies on peptide-based rod−coil block copolymer assemblies in apolar solvents are less common, although interesting properties such as organogel formation can occur due to secondary interactions of the rods.[9] This has been showcased by the work of Mezzenga and co-workers who linked an α-helical peptide to polydimethylsiloxane (PDMS) and observed network formation in toluene.[10] Herein, the apolar PDMS coil shields the polar peptide rods from the solvent and a gel is formed by the interactions between the α-helices.

Recently, we and others showed that homogeneous and predictable self-assembled structures are difficult to obtain in solution when the block co-oligomers (BCOs) are not discrete in length.[11−13] Likewise, a discrete BCO design ($Đ$ = 1) is beneficial to obtain highly organized nanostructures and small feature sizes in bulk materials, induced by phase segregation of the incompatible blocks.[14−16] The combination of interaction parameters (χ), length, and composition of the BCO gives rise to a variety of morphologies.[17−19] One of our groups showed that high incompatibility between the two parts of BCOs could be achieved by using oligodimethylsiloxane (*o*DMS) as one of

Received: January 28, 2021
Published: March 4, 2021

https://dx.doi.org/10.1021/jacs.1c01076
J. Am. Chem. Soc. 2021, 143, 4032−4042

the discrete blocks, giving rise to highly ordered structures at low degrees of polymerization.[15] Solely lamellar structures were obtained when crystallinity is introduced as an additional driving force for assembly next to phase segregation.[20] Generally, the long-range order of the lamellar structures increased upon crystallization of low molecular weight BCOs.[21,22] In analogy, peptide rod−coil BCPs favor lamellar (zigzag) structures in the bulk originating from the strong rod−rod interactions.[23−26] In the formation of these nanostructures, monodispersity is very important to obtain ordered lamellae with a sharp interface between the blocks.[27]

Oligomers of the amino acid L-proline (Pro) adopt well-defined, helical secondary structures.[28−30] These left-handed polyproline II (PPII) helices are, together with α-helices and β-sheets, the most abundant secondary structures in peptides and proteins.[31−34] Already at a length of six consecutive Pro residues, a stable PPII helix is formed.[28,29] This helix is pseudo-C_3 symmetric along the central screw axis with a helical pitch of ∼1 nm and 3 Pro residues per turn.[35,36] Due to their well-defined and rigid conformation, and the possibility to functionalize them, oligoprolines (*o*Pro) can be used as molecular rulers or scaffolds to bring two or more attached entities in a defined distance to each other.[37] This concept has been broadly applied using oligoproline conjugates for, e.g., tumor targeting,[38] light harvesting,[39,40] or in organic electronics.[41] Due to the low solubility in apolar organic solvents, most of the studies on oligoprolines have been performed in either water or polar organic solvents.[37,42−45] Yet, especially for the use of oligoprolines in supramolecular assemblies, where weak interactions such as van der Waals interactions or hydrogen bonding (H-bonding) are the main contributors, the use of noncompeting, apolar environments is highly desired.[46,47]

In contrast to other peptides, short-chain oligoprolines have no tendency to self-assemble since they lack hydrogen bond (H-bond) donors on the peptide backbone.[30] Recently, one of our groups succeeded to obtain crystal structures of an oligoproline hexamer[35] and a metal−organic framework (MOF) based on an oligoproline hexamer ligand.[48] In these two solid-state structures, neighboring oligoprolines interact by London dispersion and dipole−dipole interactions with each other (Figure 1A), either across their full lengths or segments when the oligoprolines are shifted relative to each other. Further, in the crystal structure of the oligoproline hexamer, the distance between the C-terminal H-bond donor is indicative of a H-bond with the amide carbonyl oxygen of a neighboring oligoproline (Figure 1B).[35] van der Waals interactions are also the driving force for aggregation of polymers of proline (> ∼ 100 units) into large aggregates or films at temperatures above 60 °C in water.[49−51] Little is known, however, about the assembly properties of oligoprolines in apolar solvents. In apolar environments, oligoprolines can adopt a PPI helix, a conformation that is more compact and less symmetric than the PPII helix and in which all amide bonds are *cis*.[52] We envisioned that a study of oligoprolines in apolar organic media would allow us to explore the interplay between phase segregation and aggregation, for assembly processes in solution and in the bulk.

Taking inspiration from the intriguing assembly properties of oligoproline and interest in their interactions in apolar environments, we here covalently attached hydrophilic oligoprolines of different lengths to hydrophobic siloxane oligomers to form discrete block co-oligomers (BCOs) of

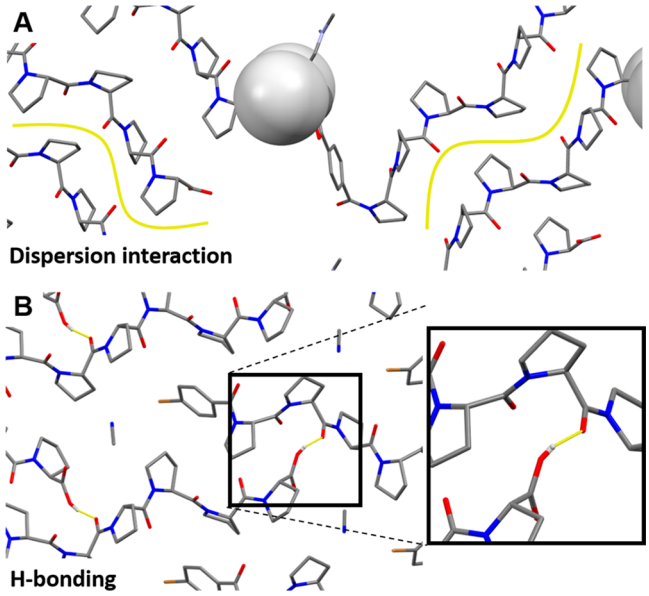

Figure 1. Crystal structures of an (A) oligoproline-based metal organic framework[48] and (B) 4-BrC_6H_4−CO-Pro$_6$−OH.[35] Van der Waals interactions (A) and hydrogen bonding (H-bonding) (B) between adjacent oligoproline helices are highlighted in yellow.

oligodimethylsiloxane-oligoprolines (*o*DMS-*o*Pro). We study the induction of microphase segregation of the two blocks, both in bulk and solution. This gave rise to assemblies of the rod−coil BCOs and allowed us to study the supramolecular aggregation of oligoproline. The structure of oligoproline can be easily modified and therefore enabled us to study how seemingly subtle changes at the molecular level manifest themselves at the supramolecular level. We analyzed the assembled structures using X-ray scattering, circular dichroism (CD) spectroscopy, transmission electron microscopy (TEM) and light scattering. With this, a thorough structural analysis of the aggregation of oligoproline in the apolar environment of siloxane oligomers was established.

RESULTS AND DISCUSSION

Design and Synthesis of Oligodimethylsiloxane-Oligoprolines. We synthesized a series of discrete di- and triblock co-oligomers consisting of oligodimethylsiloxane and L-oligoproline blocks in which the *o*DMS fraction is kept constant while the length of the *o*Pro is varied (Scheme 1). For the diblock co-oligomers, we chose a siloxane length of 15 repeating units, while the triblock co-oligomers contain a siloxane oligomer of 40 repeating units. The mono- and dihydride functionalized *o*DMS blocks were obtained from the robust synthetic strategy for the synthesis of discrete *o*DMS described in previous work (Scheme 2).[53] Proline oligomers with an *N*-terminal 5-hexenoic acid residue were obtained by standard solid phase peptide synthesis (Scheme 2 and Scheme S1). Cleavage from the resin with trifluoroacetic acid (TFA) followed by removal of TFA by ion exchange yielded the peptides with 3, 6, or 9 proline units in 36−75% yields. We varied the *o*Pro length as the Pro 6-mer and 9-mer are expected to form a PPII helix in bulk and solution, while the trimer is less prone to form the helical structure.[30,42] The oligoproline and siloxane chain were linked via platinum-catalyzed hydrosilylation (Scheme S2). With this variety of siloxane and proline oligomer lengths, we address a wide range of siloxane

https://dx.doi.org/10.1021/jacs.1c01076
J. Am. Chem. Soc. 2021, 143, 4032−4042

Scheme 1. Molecular Structures of *o*DMS$_{15}$-Pro$_n$-NH$_2$, *o*DMS$_{15}$-Pro$_n$-OMe, and *o*DMS$_{40}$-[Pro$_n$-NH$_2$]$_2$ Block Co-Oligomers (BCO)[a]

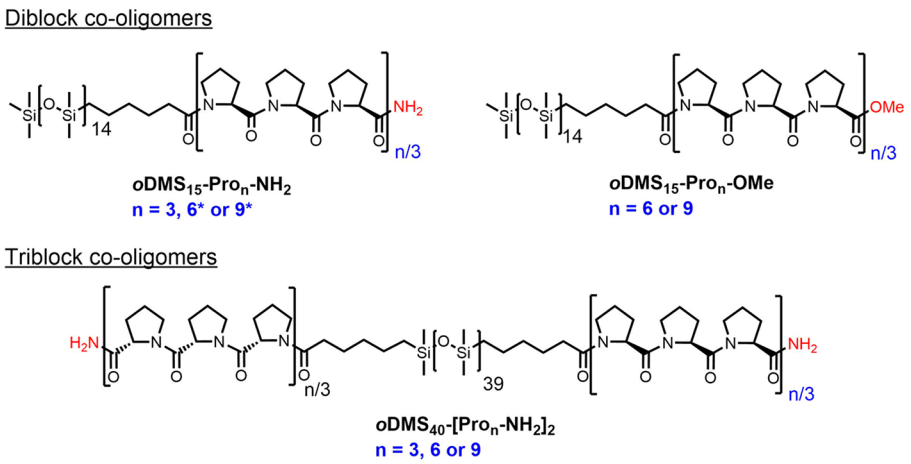

[a]The oligomers with the number n indicated with an asterisk (*) were also synthesized as the enantiomeric D-proline BCOs.

Scheme 2. Synthesis of *o*DMS$_{15}$-Pro$_9$-NH$_2$ from Hexamethylcyclotrisiloxane and Proline Starting Materials[a]

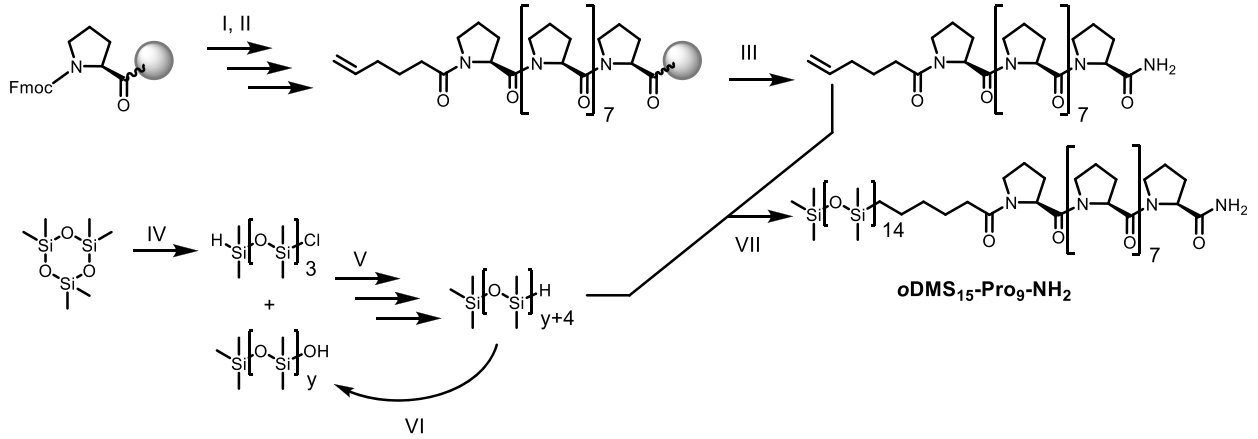

[a]The oligoproline building blocks were prepared on Rink Amide or 2-chlorotrityl chloride resin. (I) 40% piperidine in DMF, r.t., 1 × 5 min, 1 × 10 min; (II) Fmoc-Pro-OH or 5-hexenoic acid, HATU, ^{i}Pr$_2$NEt, DMF, r.t., 90 min; (III) TFA/CH$_2$Cl$_2$/H$_2$O/^{i}Pr$_3$SiH (90:5:2.5:2.5), r.t., 1 × 60 min, 1 × 30 min; (IV) chlorodimethylsilane, acetonitrile, DMF (cat.), r.t., 70 h.; (V) pyridine, toluene, r.t., 3 h; (VI) Pd/C, dioxane, 1 M phosphate buffer (pH = 7), r.t., 20 h; (VII) Karstedt's catalyst, CH$_2$Cl$_2$, 1 h.

volume fractions (f_{si} = 0.62−0.85). In addition, the functional group at the C-terminus was varied between an amide (Pro$_n$-NH$_2$) and a methyl ester (Pro$_n$-OMe) for some of the diblock co-oligomers to evaluate the effect of the C-terminal group on the supramolecular assembly. Furthermore, the enantiomeric D-proline BCO of the amide terminated diblock co-oligomers were synthesized. The resulting BCOs were obtained in high purity as confirmed by NMR spectroscopy and MALDI-ToF spectrometry (Figure 2, Figures S1−S8). The BCOs containing proline trimers (***o*DMS$_{15}$-Pro$_3$-NH$_2$** and ***o*DMS$_{40}$-[Pro$_3$-NH$_2$]$_2$**) are pastes while the BCOs with six and nine proline residues are semicrystalline solids.

The covalent attachment of a siloxane oligomer to the oligoproline resulted in good solubility of all tri- and di-BCOs in solvents such as dichloromethane and methanol. The BCOs also dissolved in apolar methylcyclohexane (MCH), even at concentrations of 10 mg mL^{-1}. Hence, they can be extensively analyzed in apolar media (*vide infra*). In contrast, the triblock co-oligomers did not dissolve in MCH, presumably due to the imbalance between the apolar *o*DMS and polar *o*Pro fraction.

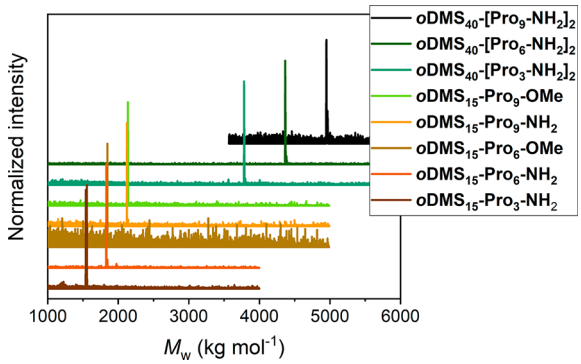

Figure 2. MALDI-ToF MS spectra of the eight *o*DMS-*o*Pro BCOs synthesized.

Interestingly, at 10 mg mL^{-1}, most diblock co-oligomers gave clear, nonviscous solutions but ***o*DMS$_{15}$-Pro$_6$-NH$_2$** formed a gel (Figure S9).

https://dx.doi.org/10.1021/jacs.1c01076
J. Am. Chem. Soc. 2021, 143, 4032−4042

Nanostructures of *o*DMS-*o*Pro BCOs in Bulk. In order to address the bulk material properties of all BCOs, their morphologies were investigated by medium- and wide-angle X-ray scattering (MAXS and WAXS). First, the morphology of the triblock co-oligomers was examined. Their 1D transmission scattering profiles are shown in Figure 3. The scattering profile

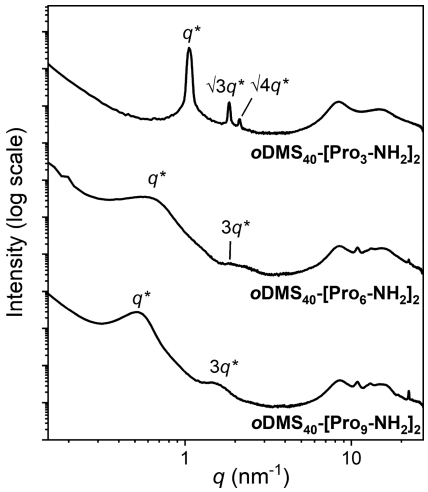

Figure 3. 1D transmission scattering profiles of $o\mathbf{DMS}_{40}$-$[\mathbf{Pro}_3\text{-}\mathbf{NH}_2]_2$ (top), $o\mathbf{DMS}_{40}$-$[\mathbf{Pro}_6\text{-}\mathbf{NH}_2]_2$ (middle), and $o\mathbf{DMS}_{40}$-$[\mathbf{Pro}_9\text{-}\mathbf{NH}_2]_2$ (bottom).

of $o\mathbf{DMS}_{40}$-$[\mathbf{Pro}_3\text{-}\mathbf{NH}_2]_2$ shows reflections at q^*, $\sqrt{3}q^*$, and $\sqrt{4}q^*$ in the MAXS region ($q < 7$ nm^{-1}), demonstrative for a hexagonally packed cylindrical phase. The absence of sharp scattering peaks in the wide-angle (WAXS) region ($q > 7$ nm^{-1}) indicates that the ordered structure is fully amorphous and originates from phase segregation. This is confirmed by the presence of an order−disorder transition temperature rather than crystallization and melting transitions (Figure S10). The 1D transmission scattering profiles of $o\mathbf{DMS}_{40}$-$[\mathbf{Pro}_6\text{-}\mathbf{NH}_2]_2$ and $o\mathbf{DMS}_{40}$-$[\mathbf{Pro}_9\text{-}\mathbf{NH}_2]_2$ show broad reflection peaks at integer multiples of q^*, representative for a lamellar packing (Figure 3). A crystalline packing of the Pro_6 and Pro_9 in the BCOs was confirmed by the presence of sharp reflection peaks in the WAXS region ($q > 7$ nm^{-1}). The scattering reflections appear at 10.9, 12.8, and 22.1 nm^{-1}, suggesting a crystalline PPII helix.[35] The crystallinity of the materials combined with the independence of the morphology on the volume fraction of siloxane indicates a breakout, crystallization-driven assembly for the triblock co-oligomers containing 6 or 9 Pro residues.

X-ray scattering experiments also provided insight into the bulk nanostructure of the di-BCOs (Figure 4). The 1D transmission scattering profile of $o\mathbf{DMS}_{15}$-$\mathbf{Pro}_3$-$\mathbf{NH}_2$ has sharp scattering peaks at q^*, $\sqrt{3}q^*$, and $\sqrt{7}q^*$ in the MAXS region but no sharp scattering peaks in the WAXS region (Figure 4A). This indicates that an amorphous, ordered, phase-segregated hexagonally packed cylindrical phase is formed, similar to the triblock analogue, but with a smaller domain spacing (Table 1,

Table 1. Bulk Morphology Characterization of *o*DMS-*o*Pro Di- and Triblock Co-Oligomers

Entry	Compound[a]	M_n[b] [g mol^{-1}]	f_{Si}[c]	Phase[d]	d[d] [nm]	Helix[e]
1	$o\mathbf{DMS}_{40}$-$[\mathbf{Pro}_3\text{-}\mathbf{NH}_2]_2$	3761.2	0.85	CYL	5.9	n.o.
2	$o\mathbf{DMS}_{40}$-$[\mathbf{Pro}_6\text{-}\mathbf{NH}_2]_2$	4386.0	0.76	LAM	10.0	PPII[f]
3	$o\mathbf{DMS}_{40}$-$[\mathbf{Pro}_9\text{-}\mathbf{NH}_2]_2$	5010.8	0.69	LAM	12.0	PPII[f]
4	$o\mathbf{DMS}_{15}$-$\mathbf{Pro}_6$-OMe	1823.2	0.70	LAM	7.2	PPII
5	$o\mathbf{DMS}_{15}$-$\mathbf{Pro}_9$-OMe	2114.6	0.62	LAM	8.2	PPII
6	$o\mathbf{DMS}_{15}$-$\mathbf{Pro}_3$-$\mathbf{NH}_2$	1516.9	0.80	CYL	4.8	n.o.
7	$o\mathbf{DMS}_{15}$-$\mathbf{Pro}_6$-$\mathbf{NH}_2$	1808.2	0.71	LAM	6.8	PPII/PPI[g]
8	$o\mathbf{DMS}_{15}$-$\mathbf{Pro}_9$-$\mathbf{NH}_2$	2099.6	0.63	LAM	8.6	PPII

[a]Block co-oligomers as depicted in Scheme 1. [b]Calculated molecular weight. [c]Volume fraction of the siloxane block, calculated using bulk densities for PDMS (0.95 g mL^{-1})[15] and crystal structure of Pro_6 (1.41 g mL^{-1}).[35] [d]Morphology of nanostructure determined with SAXS at room temperature. CYL = hexagonally packed cylinders. LAM = lamellae. Domain spacing (d) calculated using $d = 2\pi/q^*$. [e]Helix formation observed by CD spectroscopy in MeOH, MCH and in the bulk. [f]PPII helix only observed in MeOH due to insolubility in MCH (Figure S14). [g]PPII helix observed in MeOH; in bulk and MCH, a combination of PPI and PPII helices is present; n.o. = not observed.

entry 6). The diblock co-oligomers containing 6 and 9 Pro residues show scattering reflections at integer multiples of q^* (Figure 4B,C). Hence, a lamellar structure is formed driven by crystallization, again like the triblock co-oligomer analogues

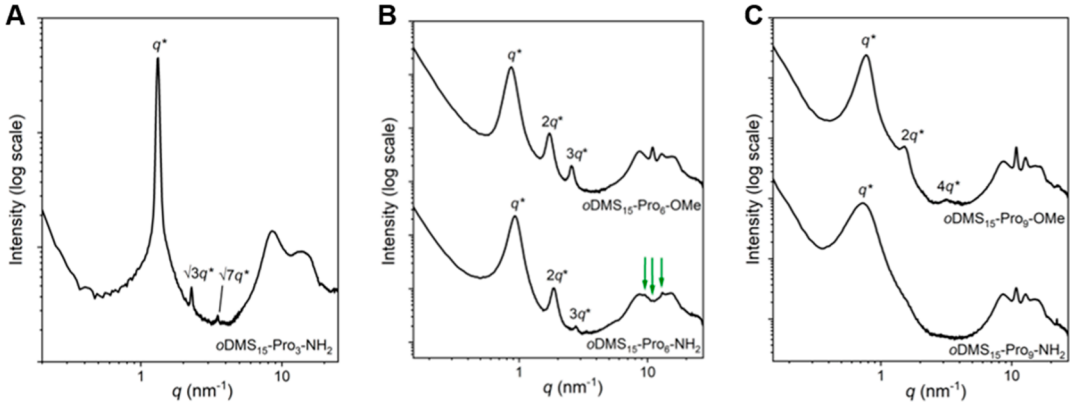

Figure 4. 1D transmission scattering profiles of (A) $o\mathbf{DMS}_{15}$-$\mathbf{Pro}_3$-$\mathbf{NH}_2$, (B) $o\mathbf{DMS}_{15}$-$\mathbf{Pro}_6$-OMe (top) and $o\mathbf{DMS}_{15}$-$\mathbf{Pro}_6$-$\mathbf{NH}_2$ (bottom), and (C) $o\mathbf{DMS}_{15}$-$\mathbf{Pro}_9$-OMe (top) and $o\mathbf{DMS}_{15}$-$\mathbf{Pro}_9$-$\mathbf{NH}_2$ (bottom).

https://dx.doi.org/10.1021/jacs.1c01076
J. Am. Chem. Soc. 2021, 143, 4032−4042

with 6 or 9 Pro residues. Moreover, the peaks in the WAXS region are at equal positions as in the respective triblock co-oligomers. Therefore, we conclude that upon an oligoproline length of six residues, the length that is enough for PPII helix formation, crystalline packing is achieved. The packing of the Pro_6 and Pro_9 moieties in the di-BCOs is identical to that in the tri-BCOs. The only exception is ***o*DMS$_{15}$-Pro$_6$-NH$_2$**, showing weak scattering peaks at different values for q, indicated with arrows in Figure 4B. Hence, the crystalline packing of ***o*DMS$_{15}$-Pro$_6$-NH$_2$** differs from that of the other BCOs, which could be an indication for the presence of a PPI helix next to a PPII helix.

Remarkably, the reflections in the MAXS region are rather broad, representing lamellar structures with a diffuse interface between the *o*DMS and *o*Pro phase. This is in stark contrast to previous work on discrete semicrystalline BCOs forming long-range, highly ordered lamellar morphologies, driven by crystallization.[20,21] In an attempt to improve the lamellar packing and long-range organization, a racemic mixture of the diblock co-oligomers was studied. Hereby, ***o*DMS$_{15}$-Pro$_9$-NH$_2$** as well as ***o*DMS$_{15}$-Pro$_6$-NH$_2$** were mixed with their D-enantiomeric BCO analogues in a 1:1 ratio. An indication of stereocomplex formation is observed by a shift of the scattering peaks in the WAXS region (Figure S11). However, the morphological ordering of the lamellae was not improved for both diblock co-oligomer stereocomplexes, represented by the broad reflection peaks of q^* and its integer multiples.

To gain more insight into the secondary structure of the L-proline block in the homochiral diblock co-oligomers, we recorded circular dichroism (CD) spectra in the bulk (Figure 5). Hereby, the BCOs were dissolved in MCH (10 mg mL^{-1})

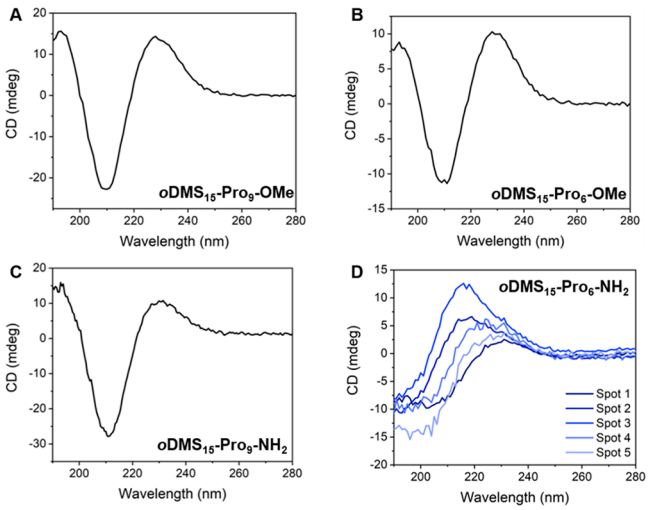

Figure 5. Solid state CD spectra of (A) ***o*DMS$_{15}$-Pro$_9$-OMe**, (B) ***o*DMS$_{15}$-Pro$_6$-OMe**, (C) ***o*DMS$_{15}$-Pro$_9$-NH$_2$** and (D) ***o*DMS$_{15}$-Pro$_6$-NH$_2$** (each line indicates a different spot on the substrate). Measured as thin film on a quartz substrate. Samples prepared from 10 mg mL^{-1} in MCH, spin-coated at 800 rpm and annealed overnight at 120 °C.

and spin-coated on a quartz substrate. After annealing at 120 °C, the resulting diblock co-oligomer films were measured at room temperature. The use of MCH as a solvent was crucial here in order to translate the assembly structure in solution (*vide infra*) to the bulk structure. In case of ***o*DMS$_{15}$-Pro$_9$-NH$_2$**, ***o*DMS$_{15}$-Pro$_6$-OMe**, and ***o*DMS$_{15}$-Pro$_9$-OMe**, the shape and intensity of the CD spectra were independent of the spot in the film where the spectrum was measured and no linear dichroism (LD) was observed in the sample (Figure S12). In addition, for these three BCOs, all CD spectra are very similar; they all show a maximum at 230 nm and minimum at 211 nm (Figures 5A–C and Figure S13A). The shape of these CD spectra is similar to that of a PPII helix (maximum at 225 nm, minimum at 207); however, the maximum and minimum shifted, which is an indication for aggregation of the PPII helical rods.[49,50] In contrast, the CD of ***o*DMS$_{15}$-Pro$_6$-NH$_2$** differed in shape and intensity when recorded at different spots of the film; a finding that shows inhomogeneity of the sample (Figure 5D and Figure S13B). These signals purely originate from a CD effect as LD can be excluded (Figure S12). These results indicate that a complex interplay of conformations and interactions causes the formation of different types and combinations of assemblies, which results in inhomogeneity of the sample and therefore a variety of CD curves. Moreover, the corresponding UV–vis spectrum of ***o*DMS$_{15}$-Pro$_6$-NH$_2$** differs from all other BCOs films, showing significant broadening of the spectrum and a shoulder at 250 nm (Figure S13). This suggests the formation of large aggregates (*vide infra*). Remarkably, ***o*DMS$_{15}$-Pro$_6$-NH$_2$** also forms a different type of crystal structure in the bulk (*vide supra*) and is the only BCO forming a gel. Therefore, we further explored these surprising results and the complex assembly of ***o*DMS$_{15}$-Pro$_6$-NH$_2$** with extensive studies in solution (*vide infra*).

The X-ray scattering analysis and the corresponding calculated domain spacings of the lamellar nanostructures allowed for a molecular packing model (Table 1). We compare the molecular packing of all BCOs, except ***o*DMS$_{40}$-[Pro$_3$-NH$_2$]$_2$** and ***o*DMS$_{15}$-Pro$_3$-NH$_2$**, as they form amorphous, cylindrical morphologies and therefore cannot be compared to the crystallization-driven, lamellar nanostructures formed by all other BCOs with 6 or more Prorepeating units. Among them, the BCOs with the same end-groups and siloxane length are compared to observe differences in packing modes related to the molecular structure. First, the methyl ester ***o*DMS$_{15}$-Pro$_6$-OMe** and ***o*DMS$_{15}$-Pro$_9$-OMe** diblock co-oligomers have a domain spacing of 7.2 and 8.2 nm, respectively (Table 1, entries 4 and 5). The difference of three oligoproline residues equals the length of ∼1 nm.[35] Hence, extending the oligoproline at a constant siloxane length gives rise to an increase of 1 nm in feature size. This finding suggests that the oligoprolines in ***o*DMS$_{15}$-Pro$_6$-OMe** and ***o*DMS$_{15}$-Pro$_9$-OMe** interface along their full length into one *o*Pro layer (Figure 6A). Second, the triblock co-oligomers ***o*DMS$_{40}$-[Pro$_6$-NH$_2$]$_2$** and ***o*DMS$_{40}$-[Pro$_9$-NH$_2$]$_2$** have a domain spacing that increases with 2 nm upon increasing the oligoproline length by three residues (∼1 nm) (Table 1, entries 2 and 3). We assume that the proline 6-mer in ***o*DMS$_{40}$-[Pro$_6$-NH$_2$]$_2$** packs in a similar fashion as ***o*DMS$_{15}$-Pro$_6$-OMe** and the increase of 2 nm in domain spacing for ***o*DMS$_{40}$-[Pro$_9$-NH$_2$]$_2$** is therefore in line with three proline residues sticking out of both sides of the *o*Pro layer, as schematically illustrated in Figure 6B. This gives rise to a diffuse interface between the *o*DMS and *o*Pro layer, evidenced by the broad scattering peaks in the 1D transmission scattering profile (Figure 3). Finally, diblock co-oligomers ***o*DMS$_{15}$-Pro$_6$-NH$_2$** and ***o*DMS$_{15}$-Pro$_9$-NH$_2$** have a domain spacing that increases with 1.8 nm upon increasing the oligoproline length with three residues. From the increase of ∼2 nm, we hypothesize a zigzag interface with three proline residues sticking out of the *o*Pro layer (Figure 6C), like the triblock co-oligomers with the same amide end-group. The

https://dx.doi.org/10.1021/jacs.1c01076
J. Am. Chem. Soc. 2021, 143, 4032–4042

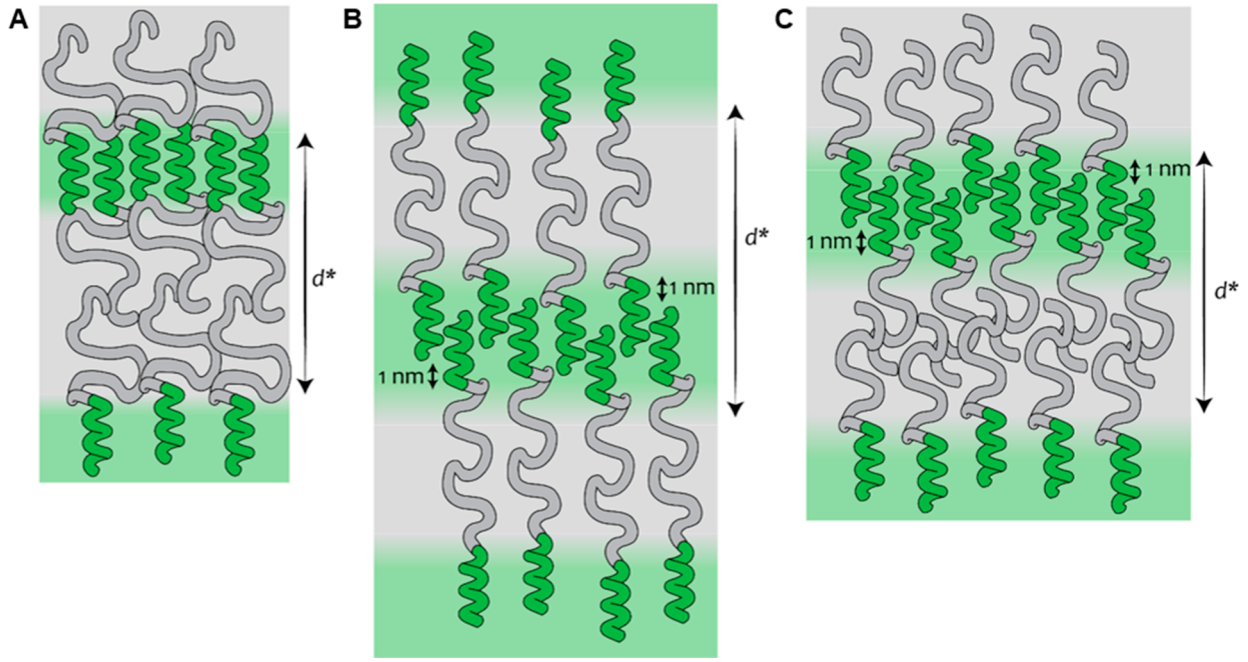

Figure 6. Schematic illustration of the BCO molecular packings showing the diffuse interface between the *o*Pro (green) and *o*DMS (gray) layers. BCOs with nine Pro repeating units are represented in the illustration. (A) Complete interdigitation of the prolines helices for ***o*DMS$_{15}$-Pro$_6$-OMe**, ***o*DMS$_{15}$-Pro$_9$-OMe**, and ***o*DMS$_{40}$-[Pro$_6$-NH$_2$]$_2$**; (B) slight interdigitation of the Pro$_9$-helices for ***o*DMS$_{40}$-[Pro$_9$-NH$_2$]$_2$**; (C) ***o*DMS$_{15}$-Pro$_9$-NH$_2$**. The domain spacing is indicated with *d**.

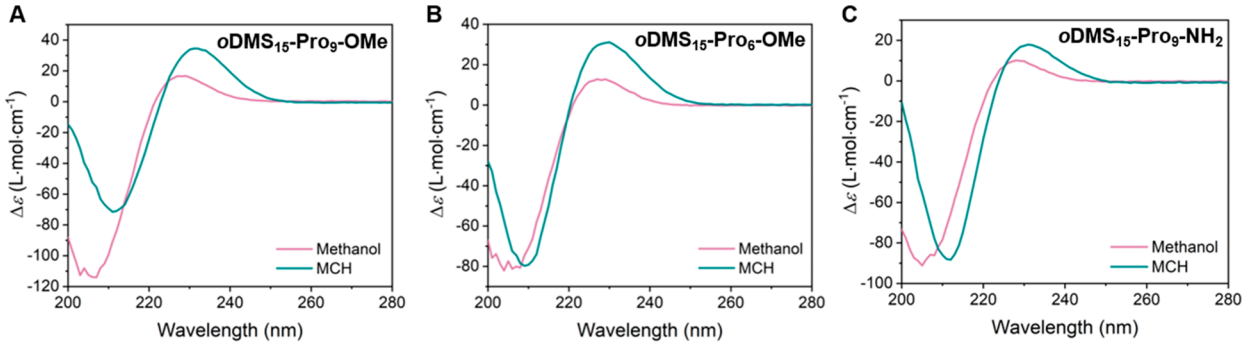

Figure 7. CD spectra of (A) ***o*DMS$_{15}$-Pro$_9$-OMe**, (B) ***o*DMS$_{15}$-Pro$_6$-OMe**, and (C) ***o*DMS$_{15}$-Pro$_9$-NH$_2$** in methanol (pink) and MCH (cyan) at 0.36 mM.

diffuse interface between the *o*DMS and *o*Pro layer for ***o*DMS$_{15}$-Pro$_9$-NH$_2$** is evidenced by the broad and single scattering peak in the 1D transmission scattering profile (Figure 4C). Again, this hypothesis is based on a packing of ***o*DMS$_{15}$-Pro$_6$-NH$_2$** that is similar to ***o*DMS$_{15}$-Pro$_6$-OMe** as a starting point, assuming complete overlap of the *o*Pro rods. However, ***o*DMS$_{15}$-Pro$_6$-NH$_2$** shows different scattering peaks in the WAXS region compared to all other BCOs (Figure 4B), indicating a different type of crystal structure, which could be a combination of PPI and PPII helices. Moreover, the presence of kinetically trapped helical structures evidenced by the thin film CD spectra (Figure 5D), in combination with the lack of a PPI crystal structure reported in literature, makes it difficult to delineate one molecular picture of ***o*DMS$_{15}$-Pro$_6$-NH$_2$** based on these results.

The difference in packing of the *o*Pro rods, based on the end-groups, is clarified by comparing ***o*DMS$_{15}$-Pro$_9$-NH$_2$** and ***o*DMS$_{15}$-Pro$_9$-OMe** both with the same proline and siloxane oligomer length. The 1D transmission scattering profiles pointed out that ***o*DMS$_{15}$-Pro$_9$-OMe** has a sharper interface between the *o*DMS and *o*Pro phase indicated by the presence of multiple and sharper scattering peaks compared to ***o*DMS$_{15}$-Pro$_9$-NH$_2$** (Figure 4C). This is in accordance with complete and partial interfacing of the *o*Pro rods in ***o*DMS$_{15}$-Pro$_9$-OMe** and ***o*DMS$_{15}$-Pro$_9$-NH$_2$**, respectively. We hypothesize that the difference in packing originates from the fact that the C-terminal amide end-group is capable of H-bonding in addition to van der Waals interactions according to the high-resolution crystal structure.[35] This additional interaction in ***o*DMS$_{15}$-Pro$_9$-NH$_2$** could equalize the enthalpy loss due to mixing of the *o*DMS and *o*Pro layer at the interface.

Aggregation of Diblock Co-Oligomers in Solution. Before we focus on the remarkable assembly behavior and properties of ***o*DMS$_{15}$-Pro$_6$-NH$_2$**, we investigated the solution assembly of the diblock co-oligomers ***o*DMS$_{15}$-Pro$_6$-OMe**, ***o*DMS$_{15}$-Pro$_9$-OMe**, and ***o*DMS$_{15}$-Pro$_9$-NH$_2$**, which all formed similar bulk assemblies. CD spectra of the diblock co-oligomers in methanol and MCH were recorded to compare the helix formation in polar and apolar solvents, respectively (Figure 7). CD spectra of the BCOs in methanol show in all three cases a

https://dx.doi.org/10.1021/jacs.1c01076
J. Am. Chem. Soc. 2021, 143, 4032−4042

minimum at 205 and a maximum at 228 nm, typical for a PPII helical peptide. In MCH, the spectra shift to higher wavelengths with a minimum at 211 nm and a maximum at 230 nm. These MCH solution-phase spectra are very similar to those observed for the BCO assembly in the bulk (*vide supra*). Hence, ***o*DMS$_{15}$-Pro$_6$-OMe**, ***o*DMS$_{15}$-Pro$_9$-OMe**, and ***o*DMS$_{15}$-Pro$_9$-NH$_2$** form PPII helices that aggregate in MCH and the bulk. Subtle broadening and lowering of the absorbance intensity in the UV−vis spectra of the BCOs in MCH compared to methanol corroborate the hypothesis (Figure S15). Formanek and co-workers have studied the aggregation of polyprolines using Fourier transform infrared (FT-IR) spectroscopy.[51] This aggregation can be explained by breaking the interactions between water molecules and the peptide carbonyl groups, thereby allowing for the interaction between polyprolines by van der Waals forces. Accordingly, we recorded FT-IR spectra of the diblock co-oligomers in the bulk material and in MCH and compared the results to those obtained in methanol where no aggregation is present. We observed a similar shift in the carbonyl region (1650 cm^{-1}) to higher wavenumbers in the bulk material and in MCH (Figure S16). H-bonding of the oligoproline carbonyls with solvent molecules is absent in MCH and in the bulk due to the apolar environment. Therefore, we infer from these results that the aggregation of the oligoproline helices in the BCOs is caused by the lack of H-bonds between the oligoproline and solvent molecules. With the similarity to previous work and the results from CD spectroscopy, our data is consistent with aggregation of the BCOs by van der Waals forces in both MCH and bulk material.

Consequences of Pathway Complexity in the Aggregation of *o*DMS-Pro$_6$-NH$_2$. The gel formation, the disparity of the CD spectra in the bulk as well as the crystal structure of ***o*DMS-Pro$_6$-NH$_2$** compared to the data obtained for the other BCOs raises questions on the assembly processes of this BCO. The findings suggest that ***o*DMS-Pro$_6$-NH$_2$** can form different types of assemblies and/or helical structures. We therefore investigated the properties of this BCO in more detail. The CD spectrum in methanol shows that ***o*DMS-Pro$_6$-NH$_2$** adopts, as the other BCOs, a PPII helix (Figure 8A). In contrast, the CD spectrum in MCH shows a broad maximum at 225 nm and is thus significantly different from the spectrum of aggregated PPII helices (*vide supra*). This spectrum is reminiscent of the spectrum typical for PPI helices that are characterized by a maximum at 213 nm and minima at 199 and 230 nm.[52] The observed signals are though significantly broader, which indicates aggregation of PPI helical and/or a coexistence of PPII helical molecules in the assemblies. To gain more insight into the assembly process and capture the effect of the oligomer length and end-group, we recorded CD spectra of ***o*DMS-Pro$_6$-NH$_2$** at various temperatures and compared them to spectra of ***o*DMS$_{15}$-Pro$_9$-NH$_2$** and ***o*DMS$_{15}$-Pro$_6$-OMe**. Interestingly, the shape of the CD spectrum of ***o*DMS$_{15}$-Pro$_6$-NH$_2$** changes upon heating to a spectrum typical for a PPII helix with a maximum and minimum at 229 and 209 nm, respectively (Figure 8B). An isosbestic point is observed indicative of the presence of two types of interconverting conformations. The CD spectrum of ***o*DMS$_{15}$-*o*Pro$_6$-NH$_2$** is at 80 °C less intense compared to the spectra of all other BCOs indicating that the emerging PPII helix is less pronounced. The CD and absorption spectra of ***o*DMS$_{15}$-Pro$_6$-OMe** (Figure 8C and Figure S17), having the same oligomer length, and of ***o*DMS$_{15}$-Pro$_9$-NH$_2$** (Figure 8D and Figure S17), having the same end-group, remained essentially the same upon heating, indicating the occurrence of PPII helices regardless of the temperature. Upon cooling at a rate of 2 K min^{-1}, identical CD spectra were observed for ***o*DMS$_{15}$-*o*Pro$_6$-NH$_2$** without hysteresis (Figure S18). Hysteresis is typical for the temperature induced transition from PPII to PPI helical oligoprolines in water and is due to slow *trans*/*cis* isomerization of the tertiary amide bonds.[54] In apolar environments, this *cis*/*trans* isomerization is significantly faster than in polar solvents,[55,56] which explains the absence of hysteresis in the interconversion of ***o*DMS$_{15}$-*o*Pro$_6$-NH$_2$** from PPI to PPII helical conformations. Here, either the MCH or the siloxane provides for the apolar environment and thus fast *cis*/*trans* isomerization.

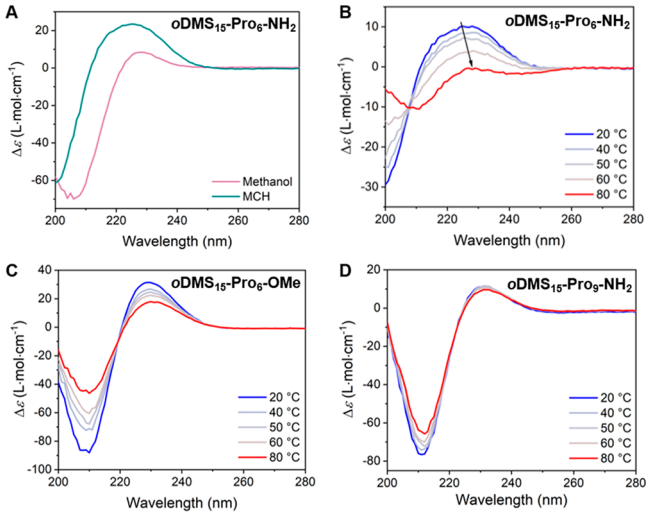

Figure 8. (A) CD spectra of ***o*DMS$_{15}$-Pro$_6$-NH$_2$** in methanol (pink) and MCH (cyan) at 0.36 mM. CD spectra of (B) ***o*DMS$_{15}$-Pro$_6$-NH$_2$**, (C) ***o*DMS$_{15}$-Pro$_6$-OMe**, and (D) ***o*DMS$_{15}$-Pro$_9$-NH$_2$** at various temperatures in MCH at 0.36 mM, measured upon heating at 2 K min^{-1}.

We measured dynamic light scattering (DLS) to better understand whether the changes in CD spectra upon heating are related to a change in the assembly state of ***o*DMS$_{15}$-*o*Pro$_6$-NH$_2$**. The aggregates of ***o*DMS$_{15}$-*o*Pro$_6$-NH$_2$** are compared to those of ***o*DMS$_{15}$-*o*Pro$_9$-NH$_2$**, which show no change in CD spectrum with varying temperature. Both BCO aggregates show an increase in diffusion coefficient with increasing temperature indicating a decrease in aggregate size (Figure 9). Most likely, the van der Waals interactions between the oligoproline rods are weakened upon heating which results in a decrease in aggregation. The increase in diffusion coefficient for ***o*DMS$_{15}$-*o*Pro$_9$-NH$_2$** is more gradual throughout the measured temperature range (20−80 °C) than observed for ***o*DMS$_{15}$-*o*Pro$_6$-NH$_2$**. The increase of the diffusion coefficient of the latter BCO is more pronounced at temperatures above 50 °C. This decrease in size is in accordance with the observed change of the CD spectrum of ***o*DMS$_{15}$-*o*Pro$_6$-NH$_2$** (Figure 8B) This observation is consistent with a conformational switch from PPI to PPII helices in case of the shorter peptide and breaking of the oligoproline rod−rod interactions of ***o*DMS$_{15}$-Pro$_9$-NH$_2$** that requires more energy than for ***o*DMS$_{15}$-Pro$_6$-NH$_2$** due to the longer *o*Pro length.

Transmission electron microscopy (TEM) gives also insight into the aggregate structure and size. We evaluated the effect of the oligoproline length and end-group on the aggregate structure and compared the aggregates of ***o*DMS$_{15}$-Pro$_6$-NH$_2$**

https://dx.doi.org/10.1021/jacs.1c01076
J. Am. Chem. Soc. 2021, 143, 4032−4042

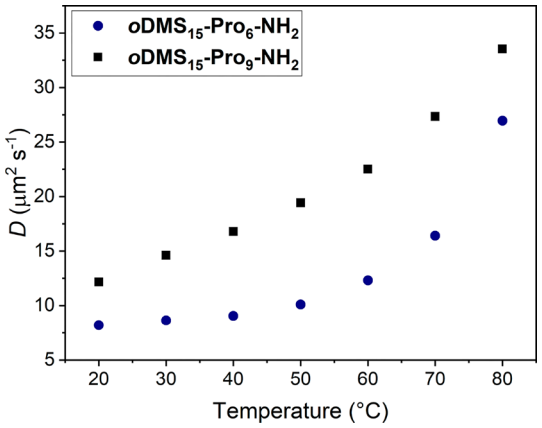

Figure 9. Diffusion coefficient as a function of temperature for ***o*DMS$_{15}$-Pro$_6$-NH$_2$** (blue rounds) and ***o*DMS$_{15}$-Pro$_9$-NH$_2$** (black squares) in MCH, 0.36 mM at 20 °C, measured by DLS.

with ***o*DMS$_{15}$-Pro$_9$-NH$_2$** and ***o*DMS$_{15}$-Pro$_6$-OMe**. A fibrillar structure is observed for ***o*DMS$_{15}$-Pro$_6$-NH$_2$** while ***o*DMS$_{15}$-Pro$_9$-NH$_2$** and ***o*DMS$_{15}$-Pro$_6$-OMe** show disperse micellar-type aggregates (Figure 10A–C). In all cases, we expect the

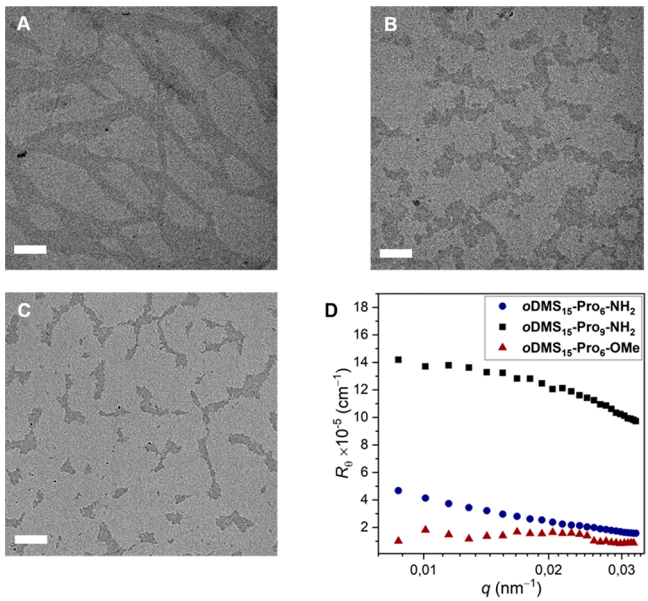

Figure 10. TEM images of (A) ***o*DMS$_{15}$-Pro$_6$-NH$_2$**, (B) ***o*DMS$_{15}$-Pro$_6$-OMe**, and (C) ***o*DMS$_{15}$-Pro$_9$-NH$_2$** in MCH, 50 μM, dried on TEM grid. Scale bar represents 200 nm. (D) Rayleigh ratio (R_θ) as a function of the wave vector (q) for ***o*DMS$_{15}$-Pro$_6$-NH$_2$** (blue rounds), ***o*DMS$_{15}$-Pro$_9$-NH$_2$** (black squares), and ***o*DMS$_{15}$-Pro$_6$-OMe** (red triangles) in MCH, 0.36 mM measured by SLS at 20 °C.

oligoprolines to be shielded by the *o*DMS from the apolar MCH solvent. The size of ***o*DMS$_{15}$-Pro$_6$-NH$_2$** aggregates is much larger than that of ***o*DMS$_{15}$-Pro$_9$-NH$_2$** and ***o*DMS$_{15}$-Pro$_6$-OMe**. This observation was confirmed by static light scattering (SLS) measurements of ***o*DMS$_{15}$-Pro$_6$-NH$_2$**, ***o*DMS$_{15}$-Pro$_9$-NH$_2$** and ***o*DMS$_{15}$-Pro$_6$-OMe** in MCH (Figure 10D). We plotted the Rayleigh ratio (R_θ) as a function of the wave vector (q) and observed a curve that is almost horizontal for ***o*DMS$_{15}$-Pro$_9$-NH$_2$** and ***o*DMS$_{15}$-Pro$_6$-OMe**. In contrast, the R_θ for ***o*DMS$_{15}$-Pro$_6$-NH$_2$** still rises toward lower q values. This increase indicates that ***o*DMS$_{15}$-Pro$_6$-NH$_2$** forms large aggregates of which the length scales are outside the regime of this scattering technique. Hence, both the scattering results and the TEM images suggest large elongated structures for ***o*DMS$_{15}$-Pro$_6$-NH$_2$** only, which most likely contribute to the network formation and is therefore proposed to be the origin of the gelation at higher concentrations.

Together, the results presented here show the complex aggregation of ***o*DMS$_{15}$-Pro$_6$-NH$_2$** in which multiple helical conformations and assembly states are present. Interestingly, this is the only BCO in this study having a different nanostructure, which alters the physical properties of the material. This is even more remarkable as the triblock oligomer ***o*DMS$_{40}$-[Pro$_6$-NH$_2$]$_2$**, with the same number of prolines and an amide end-group, does not show pathway complexity. Here, we discuss on the molecular origin of the assembly and relate the nanostructure and network formation to the gelation at higher concentration of ***o*DMS$_{15}$-Pro$_6$-NH$_2$**. The CD spectrum of ***o*DMS$_{15}$-Pro$_6$-NH$_2$** indicates the presence of both PPI and PPII helical structures at room temperature, which are most likely aggregated. The shift in maximum and minimum upon changing temperature is absent in the methyl ester analogue. This finding shows that the seemingly small structural change from a methyl ester to a primary amide or from a diblock to a triblock has a significant effect on the assembly and material properties. It indicates that ***o*DMS$_{15}$-Pro$_6$-NH$_2$** can engage not only in intermolecular van der Waals interactions but, via its C-terminal amide group, also in H-bonding with a backbone amide C=O group of a neighboring molecule, similarly to that observed in the crystal structure.[35] Thus, next to the van der Waals forces, H-bonding could be a contributing factor that guides the aggregation of ***o*DMS$_{15}$-Pro$_6$-NH$_2$** into large structures. We propose that this combination of two different helical conformations as well as an der Waals and H-bonding interactions and microphase segregation, are involved in the network formation resulting in gelation at high concentrations. The multiple interactions and conformations give rise to the pathway complexity in the supramolecular assembly. In the bulk material, in which the mobility of the BCO is virtually absent, we observe the consequence of this complex pathway selection giving rise to an inhomogeneity in the sample. Hence, there are spots in the sample in which one conformation is more populated than the other even after annealing. This indicates that the thermodynamic equilibrium is not reached for ***o*DMS$_{15}$-Pro$_6$-NH$_2$** and therefore kinetically trapped assemblies are obtained in the bulk material. The exceptional finding of pathway selection is especially remarkable in light of compound ***o*DMS$_{15}$-Pro$_9$-NH$_2$**, having the same terminal end-group, but no pathway complexity is observed. This suggests that the larger overlapping rod-length causes an increase in van der Waals forces losing the fine interplay between interactions.

CONCLUSIONS

In this work, we have investigated the assembly of siloxane-oligoproline BCOs (*o*DMS-*o*Pro) in apolar environments. The conjugation of a siloxane to an oligoproline initiates phase segregation of the rod–coil BCO in both bulk and solution, allowing for an extensive structural investigation of oligoproline aggregates in apolar media. Assembly of the *o*DMS-*o*Pro bulk material resulted in a crystallization-driven lamellar morphology with a diffuse interface between the two phases for the oligomers with at least six proline residues. The BCOs formed micellar structures in apolar solution driven by the aggregation of PPII helices via van der Waals interactions

https://dx.doi.org/10.1021/jacs.1c01076
J. Am. Chem. Soc. 2021, 143, 4032–4042

between the oligoproline rods, as expected. Surprisingly, one of the BCOs is able to form an organogel that is the result of multiple assembly pathways and conformations giving a supramolecular network. Hence, the complex interplay between aggregation forces and phase segregation gives rise to interesting material properties. With this, we have shown that subtle changes in the molecular structure, such as length and end-group, result in major differences in the supramolecular nanostructure and therefore change the physical properties of the materials. The systematic study of series of BCOs or molecules to find exceptions and explore the structure−property relationships of the supramolecular assembly is the key to the development of new material properties. Moreover, the results presented further strengthen the proposition that self-assembly processes possess pathway subtleties similar to those known in covalent chemical reactions. Therefore, treating self-assembly as noncovalent synthesis is highly desirable.[57]

■ ASSOCIATED CONTENT

Supporting Information

The Supporting Information is available free of charge at https://pubs.acs.org/doi/10.1021/jacs.1c01076.

Experimental procedures, characterization data (PDF)

■ AUTHOR INFORMATION

Corresponding Authors

Helma Wennemers − *Laboratory of Organic Chemistry, ETH Zurich, D-CHAB, 8093 Zurich, Switzerland;* orcid.org/0000-0002-3075-5741; Email: wennemers@org.chem.ethz.ch

E.W. Meijer − *Institute for Complex Molecular Systems and Laboratory of Macromolecular and Organic Chemistry, Eindhoven University of Technology, 5600 MB Eindhoven, The Netherlands;* orcid.org/0000-0003-4126-7492; Email: e.w.meijer@tue.nl

Authors

Brigitte A.G. Lamers − *Institute for Complex Molecular Systems and Laboratory of Macromolecular and Organic Chemistry, Eindhoven University of Technology, 5600 MB Eindhoven, The Netherlands*

Andreas Herdlitschka − *Laboratory of Organic Chemistry, ETH Zurich, D-CHAB, 8093 Zurich, Switzerland*

Tobias Schnitzer − *Institute for Complex Molecular Systems and Laboratory of Macromolecular and Organic Chemistry, Eindhoven University of Technology, 5600 MB Eindhoven, The Netherlands;* orcid.org/0000-0003-3613-576X

Mathijs F.J. Mabesoone − *Institute for Complex Molecular Systems and Laboratory of Macromolecular and Organic Chemistry, Eindhoven University of Technology, 5600 MB Eindhoven, The Netherlands*

Sandra M.C. Schoenmakers − *Institute for Complex Molecular Systems and Laboratory of Macromolecular and Organic Chemistry, Eindhoven University of Technology, 5600 MB Eindhoven, The Netherlands*

Bas F.M. de Waal − *Institute for Complex Molecular Systems and Laboratory of Macromolecular and Organic Chemistry, Eindhoven University of Technology, 5600 MB Eindhoven, The Netherlands*

Anja R.A. Palmans − *Institute for Complex Molecular Systems and Laboratory of Macromolecular and Organic Chemistry, Eindhoven University of Technology, 5600 MB Eindhoven, The Netherlands;* orcid.org/0000-0002-7201-1548

Complete contact information is available at: https://pubs.acs.org/10.1021/jacs.1c01076

Author Contributions

The manuscript was written through contributions of all authors. All authors have given approval to the final version of the manuscript.

Notes

The authors declare no competing financial interest.

■ ACKNOWLEDGMENTS

We thank Lafayette N. J. de Windt and dr. Gijs M. ter Huurne for the initial SLS and DLS experiments. The work in Eindhoven is funded by the Dutch Ministry of Education, Culture and Science (Gravity program 024.001.035) and the Alexander von Humboldt Foundation. T.S. thanks the Swiss National Science Foundation for a Postdoc.Mobility scholarship. The work in Zurich was funded by ETH Research Grant ETH-35 17-2.

■ REFERENCES

(1) Hendricks, M. P.; Sato, K.; Palmer, L. C.; Stupp, S. I. Supramolecular Assembly of Peptide Amphiphiles. *Acc. Chem. Res.* **2017**, *50* (10), 2440−2448.

(2) Mai, Y.; Eisenberg, A. Self-Assembly of Block Copolymers. *Chem. Soc. Rev.* **2012**, *41* (18), 5969−5985.

(3) Lee, M.; Cho, B. K.; Zin, W. C. Supramolecular Structures from Rod-Coil Block Copolymers. *Chem. Rev.* **2001**, *101* (12), 3869−3892.

(4) Carlsen, A.; Lecommandoux, S. Self-Assembly of Polypeptide-Based Block Copolymer Amphiphiles. *Curr. Opin. Colloid Interface Sci.* **2009**, *14* (5), 329−339.

(5) Cai, C.; Lin, J.; Lu, Y.; Zhang, Q.; Wang, L. Polypeptide Self-Assemblies: Nanostructures and Bioapplications. *Chem. Soc. Rev.* **2016**, *45* (21), 5985−6012.

(6) Lim, Y. B.; Moon, K. S.; Lee, M. Rod-Coil Block Molecules: Their Aqueous Self-Assembly and Biomaterials Applications. *J. Mater. Chem.* **2008**, *18* (25), 2909−2918.

(7) Wu, D.; Huang, Y.; Xu, F.; Mai, Y.; Yan, D. Recent Advances in the Solution Self-Assembly of Amphiphilic "rod-Coil" Copolymers. *J. Polym. Sci., Part A: Polym. Chem.* **2017**, *55* (9), 1459−1477.

(8) Yoon, Y. R.; Lim, Y. B.; Lee, E.; Lee, M. Self-Assembly of a Peptide Rod-Coil: A Polyproline Rod and a Cell-Penetrating Peptide Tat Coil. *Chem. Commun.* **2008**, *16*, 1892−1894.

(9) Hermes, F.; Otte, K.; Brandt, J.; Gräwert, M.; Börner, H. G.; Schlaad, H. Polypeptide-Based Organogelators: Effects of Secondary Structure. *Macromolecules* **2011**, *44* (18), 7489−7492.

(10) Kotharangannagari, V. K.; Sánchez-Ferrer, A.; Ruokolainen, J.; Mezzenga, R. Thermoreversible Gel-Sol Behavior of Rod-Coil-Rod Peptide-Based Triblock Copolymers. *Macromolecules* **2012**, *45* (4), 1982−1990.

(11) Das, A.; Petkau-Milroy, K.; Klerks, G.; van Genabeek, B.; Lafleur, R. P. M.; Palmans, A. R. A.; Meijer, E. W. Consequences of Dispersity on the Self-Assembly of ABA-Type Amphiphilic Block Co-Oligomers. *ACS Macro Lett.* **2018**, *7*, 546−550.

(12) Gangloff, N.; Höferth, M.; Stepanenko, V.; Sochor, B.; Schummer, B.; Nickel, J.; Walles, H.; Hanke, R.; Würthner, F.; Zuckermann, R. N.; et al. Linking Two Worlds in Polymer Chemistry: The Influence of Block Uniformity and Dispersity in Amphiphilic Block Copolypeptoids on Their Self-Assembly. *Biopolymers* **2019**, *4* (110), e23259.

(13) Petkau-milroy, K.; Ianiro, A.; Ahn, M. M. L.; Magana, J. R.; Vleugels, M. E. J.; Lamers, B. A. G.; Tuinier, R.; Voets, I. K.; Palmans, A. R. A.; Meijer, E. W. Architecture-Dependent Interplay between

Self-Assembly and Crystallization in Discrete Block Co-Oligomers. *ACS Macro Lett.* **2020**, 6−10.
(14) Oschmann, B.; Lawrence, J.; Schulze, M. W.; Ren, J. M.; Anastasaki, A.; Luo, Y.; Nothling, M. D.; Pester, C. W.; Delaney, K. T.; Connal, L. A.; et al. Effects of Tailored Dispersity on the Self-Assembly of Dimethylsiloxane-Methyl Methacrylate Block Co-Oligomers. *ACS Macro Lett.* **2017**, *6* (7), 668−673.
(15) Van Genabeek, B.; de Waal, B. F. M.; Gosens, M. M. J.; Pitet, L. M.; Palmans, A. R. A.; Meijer, E. W. Synthesis and Self-Assembly of Discrete Dimethylsiloxane−Lactic Acid Diblock Co-Oligomers: The Dononacontamer and Its Shorter Homologues. *J. Am. Chem. Soc.* **2016**, *138* (12), 4210−4218.
(16) Van Genabeek, B.; De Waal, B. F. M.; Ligt, B.; Palmans, A. R. A.; Meijer, E. W. Dispersity under Scrutiny: Phase Behavior Differences between Disperse and Discrete Low Molecular Weight Block Co-Oligomers. *ACS Macro Lett.* **2017**, *6* (7), 674−678.
(17) Bates, C. M.; Bates, F. S. 50th Anniversary Perspective: Block Polymers-Pure Potential. *Macromolecules* **2017**, *50* (1), 3−22.
(18) Leibler, L. Theory of Microphase Separation in Block Copolymers. *Macromolecules* **1980**, *13* (10), 1602−1617.
(19) Bates, F.; Fredrickson, G. H. Block Copolymer Thermodynamics: Theory And Experiment. *Annu. Rev. Phys. Chem.* **1990**, *41* (1), 525−557.
(20) Lamers, B. A. G.; van Genabeek, B.; Hennissen, J.; de Waal, B. F. M.; Palmans, A. R. A.; Meijer, E. W. Stereocomplexes of Discrete, Isotactic Lactic Acid Oligomers Conjugated with Oligodimethylsiloxanes. *Macromolecules* **2019**, *52* (3), 1200−1209.
(21) Van Genabeek, B.; de Waal, B. F. M.; Palmans, A. R. A.; Meijer, E. W. Discrete Oligodimethylsiloxane-Oligomethylene Di- and Triblock Co-Oligomers: Synthesis and Self-Assembly and Molecular Organization. *Polym. Chem.* **2018**, *9* (20), 2746−2758.
(22) van Genabeek, B.; Lamers, B. A. G.; de Waal, B. F. M.; van Son, M. H. C.; Palmans, A. R. A.; Meijer, E. W. Amplifying (Im)perfection: The Impact of Crystallinity in Discrete and Disperse Block Co-Oligomers. *J. Am. Chem. Soc.* **2017**, *139* (42), 14869−14872.
(23) Perly, B.; Douy, A.; Gallot, B. Block Copolymers polybutadiene/poly(benzyl-L-glutamate) and polybutadiene/poly-(N5-hydroxypropylglutamine) Preparation and Structural Study by X-ray and Electron Microscopy. *Makromol. Chem.* **1976**, *177* (9), 2569−2589.
(24) Gervais, M.; Douy, A.; Gallot, B.; Erre, R. X-Ray Photoelectron Spectroscopy of ABA Polypeptide-Polybutadiene-Polypeptide Triblock Copolymers. *Polymer* **1988**, *29* (10), 1779−1783.
(25) Janssen, K.; van Beylen, M.; Samyn, C.; Scherrenberg, R.; Reynears, H. Morphology of ABA Triblock Copolymers Consisting of Poly(γ-Benzyl L-Glutamate) as the A Component and Polystyrene as the B Component. *Makromol. Chem.* **1990**, *191* (11), 2777−2785.
(26) Klok, H. A.; Lecommandoux, S. Supramolecular Materials via Block Copolymer Self-Assembly. *Adv. Mater.* **2001**, *13* (16), 1217−1229.
(27) Schlaad, H.; Smarsly, B.; Losik, M. The Role of Chain-Length Distribution in the Formation of Solid-State Structures of Polypeptide-Based Rod-Coil Block Copolymers. *Macromolecules* **2004**, *37* (6), 2210−2214.
(28) Kakinoki, S.; Hirano, Y.; Oka, M. On the Stability of Polyproline-I and II Structures of Proline Oligopeptides. *Polym. Bull.* **2005**, *53* (2), 109−115.
(29) Rabanal, F.; Ludevid, M. D.; Pons, M.; Giralt, E. CD of Proline-Rich Polypeptides: Application to the Study of the Repetitive Domain of Maize Glutelin-2. *Biopolymers* **1993**, *33* (7), 1019−1028.
(30) Zotti, M. D.; Formaggio, F.; Crisma, M.; Peggion, C.; Moretto, A.; Toniolo, C. Handedness Preference and Switching of Peptide Helices. Part I: Helices Based on Protein Amino Acids. *J. Pept. Sci.* **2014**, *20* (5), 307−322.
(31) Shi, Z.; Chen, K.; Liu, Z.; Kallenbach, N. R. Conformation of the Backbone in Unfolded Proteins. *Chem. Rev.* **2006**, *106* (5), 1877−1897.
(32) Rath, A.; Davidson, A. R.; Deber, C. M. The Structure Of "unstructured" regions in Peptides and Proteins: Role of the Polyproline II Helix in Protein Folding and Recognition. *Biopolymers* **2005**, *80* (2−3), 179−185.
(33) Stapley, B. J.; Creamer, T. P. A Survey of Left-Handed Polyproline II Helices. *Protein Sci.* **1999**, *8* (3), 587−595.
(34) Adzhubei, A. A.; Sternberg, M. J. E.; Makarov, A. A. Polyproline-II Helix in Proteins: Structure and Function. *J. Mol. Biol.* **2013**, *425* (12), 2100−2132.
(35) Wilhelm, P.; Lewandowski, B.; Trapp, N.; Wennemers, H. A Crystal Structure of an Oligoproline PPII-Helix, at Last. *J. Am. Chem. Soc.* **2014**, *136* (45), 15829−15832.
(36) Cowan, B. P. M.; Mcgavin, S. *Structure of Poly-L-Proline* **1955**, No. 4400, 501−503.
(37) Dobitz, S.; Aronoff, M. R.; Wennemers, H. Oligoprolines as Molecular Entities for Controlling Distance in Biological and Material Sciences. *Acc. Chem. Res.* **2017**, *50* (10), 2420−2428.
(38) Kroll, C.; Mansi, R.; Braun, F.; Dobitz, S.; Maecke, H. R.; Wennemers, H. Hybrid Bombesin Analogues: Combining an Agonist and an Antagonist in Defined Distances for Optimized Tumor Targeting. *J. Am. Chem. Soc.* **2013**, *135* (45), 16793−16796.
(39) Stryer, L.; Haugland, R. P. Energy Transfer: A Spectroscopic Ruler. *Proc. Natl. Acad. Sci. U. S. A.* **1967**, *58* (2), 719−726.
(40) McCafferty, D. G.; Friesen, D. A.; Danielson, E.; Wall, C. G.; Saderholm, M. J.; Erickson, B. W.; Meyer, T. J. Photochemical Energy Conversion in a Helical Oligoproline Assembly. *Proc. Natl. Acad. Sci. U. S. A.* **1996**, *93* (16), 8200−8204.
(41) Ochs, N. A. K.; Lewandowska, U.; Zajaczkowski, W.; Corra, S.; Reger, S.; Herdlitschka, A.; Schmid, S.; Pisula, W.; Müllen, K.; Bäuerle, P.; et al. Oligoprolines Guide the Self-Assembly of Quaterthiophenes. *Chem. Sci.* **2019**, *10* (20), 5391−5396.
(42) Rothe, M.; Rott, H. NMR Spectroscopic Detection of Cis and Trans Peptide Bonds in Unprotected Oligo-L-Prolines. *Angew. Chem., Int. Ed. Engl.* **1976**, *15* (12), 770−771.
(43) Best, R. B.; Merchant, K. A.; Gopich, I. V.; Schuler, B.; Bax, A.; Eaton, W. A. Effect of Flexibility and Cis Residues in Single-Molecule FRET Studies of Polyproline. *Proc. Natl. Acad. Sci. U. S. A.* **2007**, *104* (48), 18964−18969.
(44) Sahoo, H.; Roccatano, D.; Hennig, A.; Nau, W. M. A 10-Å Spectroscopic Ruler Applied to Short Polyprolines. *J. Am. Chem. Soc.* **2007**, *129* (31), 9762−9772.
(45) Garbuio, L.; Lewandowski, B.; Wilhelm, P.; Ziegler, L.; Yulikov, M.; Wennemers, H.; Jeschke, G. Shape Persistence of Polyproline II Helical Oligoprolines. *Chem. - Eur. J.* **2015**, *21* (30), 10747−10753.
(46) Hunter, C. A. Quantifying Intermolecular Interactions: Guidelines for the Molecular Recognition Toolbox. *Angew. Chem., Int. Ed.* **2004**, *43* (40), 5310−5324.
(47) Yang, L.; Adam, C.; Nichol, G. S.; Cockroft, S. L. How Much Do van Der Waals Dispersion Forces Contribute to Molecular Recognition in Solution? *Nat. Chem.* **2013**, *5* (12), 1006−1010.
(48) Schnitzer, T.; Paenurk, E.; Trapp, N.; Gershoni-Poranne, R.; Wennemers, H. Peptide-Metal Frameworks with Metal String Guided by Dispersion Interactions. *J. Am. Chem. Soc.* **2021**, *143* (2), 644−648.
(49) Tooke, L.; Duitch, L.; Measey, T. J.; Schweitzer-Stenner, R. Kinetics of the Self-Aggregation and Film Formation of Poly-L-Proline at High Temperatures Explored by Circular Dichroism Spectroscopy. *Biopolymers* **2010**, *93* (5), 451−457.
(50) Lorusso, M.; Pepe, A.; Ibris, N.; Bochicchio, B. Molecular and Supramolecular Studies on Polyglycine and Poly-L-Proline. *Soft Matter* **2011**, *7* (13), 6327−6336.
(51) Swenson, C. A.; Formanek, R. Infrared Study of Poly-L-Proline in Aqueous Solution. *J. Phys. Chem.* **1967**, *71* (12), 4073−4077.
(52) Kuemin, M.; Schweizer, S.; Ochsenfeld, C.; Wennemers, H. Effects of Terminal Functional Groups on the Stability of the Polyproline II Structure: A Combined Experimental and Theoretical Study. *J. Am. Chem. Soc.* **2009**, *131* (42), 15474−15482.
(53) Lamers, B. A. G.; Waal, B. F. M.; Meijer, E. W. The iterative synthesis of discrete dimethylsiloxane oligomers: A practical guide. *J. Polym. Sci.* **2020**, DOI: 10.1002/pol.20200649.

https://dx.doi.org/10.1021/jacs.1c01076
J. Am. Chem. Soc. 2021, 143, 4032−4042

(54) Kuemin, M.; Engel, J.; Wennemers, H. Temperature-Induced Transition between Polyproline I and II Helices: Quantitative Fitting of Hysteresis Effects. *J. Pept. Sci.* **2010**, *16*, 596−600.
(55) Siebler, C.; Maryasin, B.; Kuemin, M.; Erdmann, R. S.; Rigling, C.; Grünenfelder, C.; Ochsenfeld, C.; Wennemers, H. Importance of Dipole Moments and Ambient Polarity for the Conformation of Xaa-Pro Moieties - a Combined Experimental and Theoretical Study. *Chem. Sci.* **2015**, *6* (12), 6725−6730.
(56) Egli, J.; Siebler, C.; Köhler, M.; Zenobi, R.; Wennemers, H. Hydrophobic Moieties Bestow Fast-Folding and Hyperstability on Collagen Triple Helices. *J. Am. Chem. Soc.* **2019**, *141* (14), 5607−5611.
(57) Vantomme, G.; Meijer, E. W. The Construction of Supramolecular Systems. *Science* **2019**, *363* (6434), 1396−1397.

https://dx.doi.org/10.1021/jacs.1c01076
J. Am. Chem. Soc. 2021, 143, 4032−4042